Microsolvation of the Phenol Cation (Ph^+) in Nonpolar Environments: Infrared Spectra of Ph^+-L_n (L = He, Ne, Ar, N_2, CH_4)†

Nicola Solcà and Otto Dopfer*

Institute for Physical Chemistry, University of Basel, Klingelbergstrasse 80, CH-4056 Basel, Switzerland

Received: October 31, 2000; In Final Form: January 24, 2001

Infrared photodissociation spectra of several phenol−L_n cation clusters (Ph^+-L_n; L = He, Ne, Ar, N_2, CH_4) are recorded in the vicinity of the O−H stretch vibration (ν_1) of bare Ph^+. The Ph^+-L_n complexes are produced in an electron impact (EI) ion source, which generates predominantly the most stable isomer of each cluster ion. The spectra of all dimers ($n = 1$) show strong ν_1 transitions (at 3537, 3534, 3464, 3365, 3365 cm^{-1} for L = He, Ne, Ar, N_2, CH_4), which are attributed to proton-bound structures based upon the complexation-induced redshifts, $\Delta\nu_1$. A linear correlation between $\Delta\nu_1$ and the proton affinity of L is observed. In the case of Ph^+-Ar, a weak transition at 3536 cm^{-1} is assigned to the ν_1 band of the less stable π-bound isomer. The analysis of photofragmentation branching ratios and systematic frequency shifts in the spectra of larger Ph^+-L_n clusters ($n \leq 2$ for CH_4, $n \leq 5$ for Ar, $n \leq 7$ for N_2) provide information about the microsolvation process of Ph^+ in nonpolar environments. The ν_1 transitions of the most stable isomers display small incremental blueshifts with respect to the dimer transitions, suggesting that further solvation causes little destabilization of the intermolecular proton bond to the first ligand. In the case of the $Ph^+-(N_2)_n$ complexes, the existence of two isomers is observed in the size range $n = 5-7$. For several Ph^+-L_n clusters, the most stable cation structures produced in the EI source differ considerably from the geometries observed by resonant enhanced multiphoton ionization (REMPI) of the corresponding neutral precursors. The limitations of REMPI techniques (arising from the Franck-Condon principle) for the generation and spectroscopic characterization of cluster cations are discussed.

I. Introduction

Complexes of aromatic molecules are often used as model systems to study intermolecular forces relevant for important phenomena in the areas of physics, chemistry, and biology. In particular, complexes of phenol (Ph) with simple ligands (L) are interesting because Ph offers two major competing binding sites (Figure 1): L can bind either to the π-electron system of the aromatic ring (π-bond) or to the O−H group to form a hydrogen bond (H-bond). Other binding sites are usually less stable. The preference of L for forming a π-bond or a H-bond depends strongly upon the type of ligand and the electronic excitation or charge state of Ph. For example, spectroscopic studies and ab initio calculations show that "spherical" ligands without low-order multipole moments (i.e., dipole and quadrupole moments), such as rare gas (Rg) atoms or CH_4, feature π-bound Ph−L equilibrium structures in the ground electronic state, S_0.[1−9] The attraction in these systems is mainly based upon dispersion forces between L and the π-electron system of Ph (induction is less important), which are maximized at the π-bound geometry. High-level ab initio calculations[10,11] and spectroscopy at the level of rotational resolution[12,13] have proven that the related benzene-Rg dimers have π-bound equilibrium structures with C_{6v} symmetry in S_0. In contrast to "spherical" ligands, ligands with permanent dipole and/or quadrupole moments (e.g., N_2 or CO) favor H-bonds to the acidic proton of Ph in the S_0 state, owing to electrostatic forces.[4,6,8,14−16]

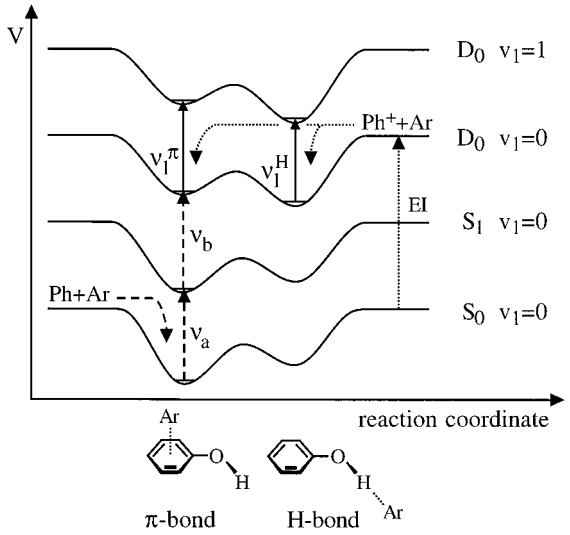

Figure 1. Sketch of potential energy diagrams of Ph−Ar in various electronic (S_0, S_1, D_0) and vibrational states ($v_1 = 0, 1$). The dashed arrows indicate the preparation of Ph^+-Ar cations in the D_0 state by resonant enhanced multiphoton ionization (REMPI): the neutral precursor is formed in a molecular beam in the S_0 state and resonantly ionized with two photons (ν_a, ν_b) via the S_1 state. The dotted arrows indicate the preparation of Ph^+-Ar cations in the D_0 state by electron impact (EI): Ph is ionized by EI, and complexes of Ph^+ with Ar are subsequently formed in the molecular beam.

Most of the spectroscopic information about the intermolecular potential in the ground electronic state of Ph^+-L cations (L = Rg, CH_4, N_2, CO), D_0, has been obtained with techniques based upon resonant enhanced multiphoton ionization (REMPI)

* Corresponding author. E-mail: otto.dopfer@unibas.ch. Phone: +41 61 267 3823. Fax: +41 61 267 3855.

† Part of the special issue "Edward W. Schlag Festschrift".

10.1021/jp004002h CCC: $20.00
Published on Web 03/29/2001

of the neutral Ph−L precursor through the first excited singlet state, S_1. Figure 1 depicts the excitation scheme for the case of Ph−Ar. Neutral Ph−L dimers are formed in a supersonic expansion and ionized by two photons either with the same ($2\nu_a$) or different frequencies (ν_a and ν_b). The techniques employed include photoionization efficiency (PIE) measurements,[2,14,16] zero kinetic energy (ZEKE) photoelectron spectroscopy,[5,7−9,14,16] mass-analyzed threshold ionization (MATI),[8,9,14,16] and the combination of REMPI with infrared (IR) photodissociation spectroscopy.[6,17] Photoionization spectra (obtained by scanning ν_b) provide detailed information about the interaction potential in the cation ground state via the measurement of binding energies, ionization energies (IE), and Franck-Condon (FC) active inter- and intramolecular modes. Additional and often complementary information about structure and bond strength of Ph^+−L dimers has been obtained by REMPI-IR spectroscopy. In particular, the complexation-induced frequency shift of the strongly IR active O−H stretch vibration (ν_1), which has small FC intensity, provides a measure of the interaction strength in H-bound Ph^+−L dimers.[6] In general, the binding energies of Ph^+−L are significantly higher than those of neutral Ph−L, due to the additional electrostatic and induction forces caused by the positive charge distribution.

In the present work, the structure and stability of several Ph^+−L dimers are investigated by IR spectroscopy. In contrast to previous studies, the cation dimers are produced in an electron impact (EI) ion source rather than by a REMPI process. Although REMPI techniques are sensitive and size-selective methods for preparing and spectroscopically probing cation complexes, they are limited by the FC principle. These limitations are briefly discussed by considering the potential curves for Ph−Ar in Figure 1. According to ab initio calculations,[7] Ph−Ar has a π-bound equilibrium structure in S_0 (in agreement with all experimental data), whereas the H-bound structure is a less stable local minimum (which has not yet been identified experimentally). Consequently, resonant photoionization of neutral Ph−Ar dimers (produced in a molecular beam) via the S_1 state leads mainly to the production of π-bound Ph^+−Ar cations in the D_0 state because the FC principle strongly favors vertical transitions (dashed arrows in Figure 1). Transitions from the π-bound to the H-bound minima (and vice versa) have nearly vanishing FC factors because they imply a large geometry change. Therefore, all transitions observed in REMPI,[1−3,7] PIE,[2] ZEKE,[5,7−9] MATI,[9] and REMPI-IR spectra[6,17] of Ph−Ar/Ph^+−Ar have been attributed to the π-bound isomer. No signature of the H-bound Ph−Ar/Ph^+−Ar isomer has been observed in these spectra, although the H-bound structure is the global minimum in the D_0 state.[18,19] The fact that H-bound Ph^+−Ar is more stable than π-bound Ph^+−Ar leads also to the important consequence that the IE of Ph−Ar determined by ZEKE/MATI spectroscopy is clearly not the adiabatic IE (as stated in refs 7 and 9). In the present work, the limitations of using REMPI techniques to prepare and probe cluster ion structures are overcome by generating Ph^+−L_n in an EI cluster ion source.[18,19] As will be outlined in more detail in section II, this ion source produces mainly the most stable isomer of a given cluster ion. In the case of Ph^+−Ar (see Figure 1), Ph is ionized first by EI, and Ph^+−Ar dimers are subsequently produced by three-body association reactions (dotted arrows in Figure 1). As H-bound Ph^+−Ar is more stable than π-bound Ph^+−Ar, the abundance of the former isomer in the EI source is larger. Indeed, both isomers have unambiguously been identified by IR spectroscopy on the basis of their characteristic O−H stretch frequency.[18,19] As expected, the relative abundance of the less stable π-bound Ph^+−Ar isomer depends strongly upon the expansion conditions.[19] Similar to Ph^+−Ar, the H-bound structure of Ph^+−N_2 is calculated to be more stable than the π-bound structure.[15,18] Experimentally, only the H-bound structure has been observed in both the REMPI[6,14,16] and EI sources.[18] In contrast to Ph^+−Ar, the REMPI techniques have no limitations in the case of Ph^+−N_2, as the H-bound structure is the global minimum on the intermolecular potential in all considered electronic states (S_0, S_1, D_0).

In the present work, IR spectra of Ph^+−L with L = He, Ne, and CH_4 are presented for the first time. In analogy to Ph^+−Ar, the H-bound structure is expected to be the global minimum for these dimers. Moreover, as the polarizability of L, α_L, increases in the order He < Ne < Ar < CH_4, the bond strength and the complexation-induced redshift in the O−H stretch fundamental, $\Delta\nu_1$, are anticipated to vary in the same order. Previous studies of H-bound AH^+−Rg dimers revealed a strong correlation between $\Delta\nu_1$ and α_{Rg}.[20,21] The quadrupole moment of N_2 provides additional contributions to the stabilization energy in Ph^+−N_2, the amount of which can be estimated from the deviation of the $\Delta\nu_1$ vs α_L relation established from L = Rg and CH_4. In addition to dimers, spectra of larger Ph^+−L_n complexes ($n \leq 2, 5, 7$ for L = CH_4, Ar, N_2) are recorded to investigate the microsolvation of Ph^+ in simple nonpolar environments. Previous IR spectroscopic studies for a variety of related AH^+−L_n systems (e.g., H_2O^+−Ar_n,[22] NH_4^+−Ar_n,[23] HCO^+−Ar_n,[24] $SiOH^+$−Ar_n,[20] N_2H^+−Ar_n,[25] N_2H^+−Ne_n,[26] CH_3^+−Ar_n[27]) provided detailed insight into the cluster growth (e.g., ligand binding energies, formation of solvation shells, existence of isomers) via the analysis of size-dependent photofragmentation branching ratios and vibrational frequency shifts. In the case of larger Ph^+−L_n clusters (L = N_2, Ar, CH_4), only Ph^+−Ar_2 has been investigated by spectroscopy prior to the present study. The additivity of the shifts in the S_1 and D_0 origins upon sequential Ar complexation observed in photoionization spectra (REMPI, PIE) has been taken as evidence that the structure of the observed isomer, denoted (1|1), is one in which two equivalent π-bound Ar ligands are attached on opposite sites to the aromatic Ph ring (C_s symmetry).[2,28] The present work demonstrates that this structure is, however, only a local minimum of the Ph^+−Ar_2 trimer cation.

II. Experimental Section

IR photodissociation spectra of mass-selected Ph^+−L_n complexes are recorded in a tandem mass spectrometer described in detail previously.[24,29] A heated Ph sample ($T \approx 330$ K) is seeded in the desired ligand gas (L = He, Ne, Ar, N_2, CH_4) at backing pressures of 6−15 bar and expanded through a pulsed nozzle into a vacuum chamber. EI ionization of the gas mixture is accomplished by electron beams emitted from two tungsten filaments close to the nozzle orifice. Several production mechanisms for Ph^+−L_n complexes may compete in such a source, and their importance depends on the experimental parameters, e.g., the position of EI ionization with respect to the collision region of the supersonic expansion. The following three processes are considered. (i) Neutral Ph−L_n complexes are first produced and then ionized. (ii) Larger neutral Ph_j−L_k clusters ($j \geq 1$ and/or $k \geq$ n) are generated and ionized, and Ph^+−L_n clusters are produced by evaporative cooling. (iii) Ph molecules are first ionized, and the produced Ph^+ cations serve then as seed ions for subsequent three-body association reactions to generate Ph^+−L_n. The following experimental observations

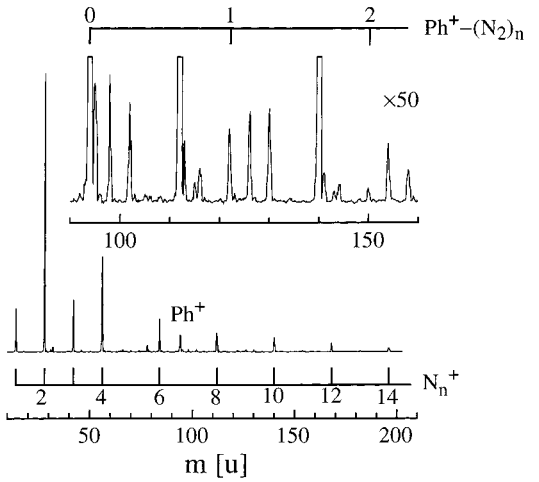

Figure 2. Mass spectrum of the electron impact cluster ion source for an expansion of heated Ph vapor seeded in N_2 (6 bar backing pressure). The mass spectrum is dominated by N_n^+ (with strong even/odd alternation) and Ph^+. Only little fragmentation of Ph is observed upon EI ionization. Major cluster ion series are $X^+-(N_2)_n$, with X = N_2 or Ph, and the impurities O_2 and H_2O.

identify process iii as the dominant mechanism for Ph^+-L_n formation under the present ion source conditions. The intensities of Ph^+-L_n clusters in mass spectra of the source decrease rapidly with n (Figure 2). Moreover, the mass spectra show no structure owing to magic numbers. Both observations are taken as evidence that Ph^+-L_n clusters are produced by stepwise aggregation (process iii) rather than by fragmentation of larger clusters (process ii). In addition, the efficiency for cluster production decreases rapidly when EI occurs further downstream in the collision-free region of the molecular beam, i.e., when neutral complexes are first formed and then ionized (processes i and ii). In conclusion, all observations are consistent with the assumption that EI ionization of Ph close to the nozzle orifice and subsequent clustering reactions with ligands L via three-body collisions are the main route for the production of Ph^+-L_n clusters in the present ion source (process iii)

$$Ph + e^- \rightarrow Ph^+ + 2e^- \quad (1a)$$

$$Ph^+-L_{n-1} + L + M \rightarrow Ph^+-L_n + M \ (M = L \text{ or } Ph) \quad (1b)$$

As an important consequence of this production scheme, the ion source generates predominantly the most stable isomer of a given cluster cation (which might have a rather different geometry than the most stable structure of the neutral species). Figure 2 shows a typical mass spectrum of the ion source for L = N_2. The dominant ions are N_n^+ (with strong n = even/odd intensity alternation) and $Ph^+-(N_2)_n$. Impurities of H_2O and O_2 give rise to the production of $H_2O^+-(N_2)_n$ and $O_2^+-(N_2)_n$. In addition, little fragmentation of Ph upon EI ionization is observed.

The central part of the plasma is extracted through a skimmer into a first quadrupole mass spectrometer (QMS1) to select the cluster ions under investigation, Ph^+-L_n. The mass-selected parent beam is then injected into an octopole ion guide, where it is overlapped with a counter propagating IR laser pulse. Single-photon absorption of mid-IR radiation in the 3 μm spectral range ($\nu \approx 3.5 \times 10^3$ cm^{-1}) leads to resonant excitation of vibrational levels of Ph^+-L_n above the threshold for ligand evaporation, resulting in the following photodissociation scheme:

$$Ph^+-L_n + h\nu \rightarrow (Ph^+-L_n)^* \rightarrow Ph^+-L_m + (n-m)L \quad (2)$$

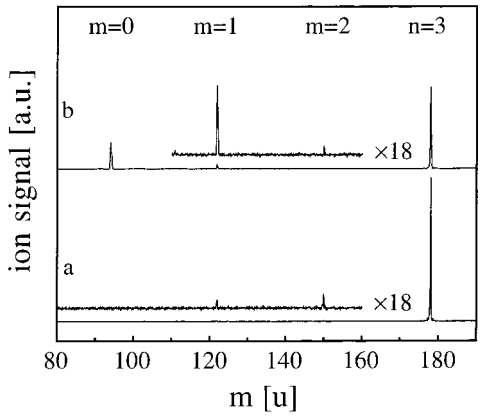

Figure 3. Mass spectrum obtained by mass-selecting $Ph^+-(N_2)_3$ with QMS1 and scanning QMS2. In case a, the laser is off, and the observed $Ph^+-(N_2)_m$ fragment ions (m = 1, 2) arise from metastable decay (MD) and/or collision-induced dissociation (CID). In case b, the laser is tuned to a resonance of $Ph^+-(N_2)_3$, ν_1 = 3381 cm^{-1}, leading to additional fragmentation into the m = 0 and 1 daughter channels (laser-induced dissociation, LID).

As expected, only the rupture of the weak intermolecular bonds is observed at the laser intensities and wavelengths employed. The produced Ph^+-L_m fragment ions are selected by a second quadrupole mass spectrometer (QMS2) and monitored by a Daly ion detector as a function of the laser frequency to obtain the IR action spectrum of Ph^+-L_n. For larger clusters ($n \geq 2$), several fragment channels (m) can occur. In these cases, action spectra are recorded simultaneously in the two major fragment channels. In general, the spectra recorded in different fragment channels are similar. The spectra shown in the figures are those obtained in the dominant fragment channel. As an example, Figure 3 shows the mass spectra obtained by mass-selecting $Ph^+-(N_2)_3$ with QMS1 and scanning QMS2 without (a) and with (b) resonant IR excitation. The mass spectrum in Figure 3a shows a strong parent peak (n = 3) and weak signals in the m = 1 and m = 2 fragment channels (<1%) arising from metastable decay (MD) of hot parent clusters and/or collision-induced dissociation (CID) caused by background gas in the octopole. The mass spectrum in Figure 3b (laser on, ν = 3381 cm^{-1}) reveals additional fragmentation of the n = 3 cluster, owing to resonant laser-induced dissociation (LID) into the m = 0 (90%) and m = 1 (10%) fragment channels. In total, ≈30% of $Ph^+-(N_2)_3$ is depleted by the LID process. To distinguish between LID and MD/CID signals, we triggered the ion source at twice the laser frequency (20 Hz) and subtracted the signals from alternate triggers. Only for small clusters, the LID signals interfere with the MD/CID background signals. For larger clusters ($n \geq 3$), LID leads in all cases to the evaporation of more than two ligands, whereas MD and CID processes mainly produce $m = n - 1$ and $m = n - 2$ daughter ions (e.g., see Figure 3 for L = N_2 and n = 3).

Tunable IR radiation is generated by a pulsed optical parametric oscillator laser system (bandwidth 0.02 cm^{-1}, 2500−6900 cm^{-1} tuning range, 0.5−5 mJ/pulse) pumped by a Nd:YAG laser. Frequency calibration (accurate to <0.2 cm^{-1}) is accomplished by recording optoacoustic spectra of NH_3 simultaneously with the action spectra.[30]

III. Results and Discussion

A. Ph^+-L Dimers (n = 1). Figure 4 reproduces the IR photodissociation spectra of several Ph^+-L dimers (L = He, Ne, Ar, CH_4, N_2) recorded in the vicinity of the O−H stretch fundamental of bare Ph^+ (ν_1 = 3534 cm^{-1}).[6] The observed band

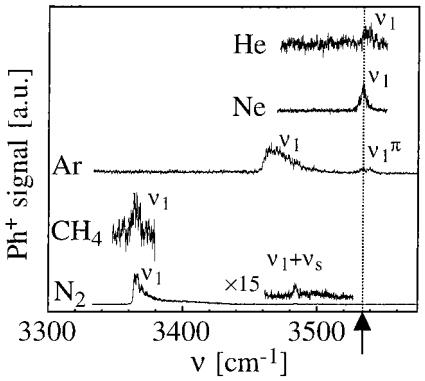

Figure 4. IR photodissociation spectra of Ph^+-L dimers (L = He, Ne, Ar, CH_4, N_2) recorded in the Ph^+ fragment channel. The strongest band in each spectrum is attributed to the ν_1 fundamental of the H-bound structure (ν_1). In the case of Ph^+-Ar, the ν_1 transition of the less stable π-bound isomer is also observed (ν_1^{π}). A weak transition in the Ph^+-N_2 spectrum is assigned to the $\nu_1 + \nu_s$ combination band of the H-bound structure. The arrow and dotted line indicate the ν_1 frequency of bare Ph^+ ($\nu_1 = 3534$ cm^{-1}).

TABLE 1: Band Maxima, Widths (fwhm, in parentheses), and Assignments of the Transitions Observed in the IR Photodissociation Spectra of Ph^+-L_n Recorded in the Dominant Fragment Channel

L	*n*	ν [cm^{-1}]	assignment	L	*n*	ν [cm^{-1}]	assignment
He	1	3537 (8)	ν_1	N_2	1	3365 (4)	ν_1
Ne	1	3534 (6)	ν_1		1	3484 (4)	$\nu_1+\nu_s$
Ar	1	3464 (12)	ν_1		2	3375 (10)	ν_1
	1	3536 (10)	ν_1^{π}		2	3488 (5)	$\nu_1+\nu_s$
	2	3467 (15)	ν_1		3	3381 (10)	ν_1
	3	3470 (13)	ν_1		4	3384 (15)	ν_1
	4	3475 (15)	ν_1		5	3387 (12)	ν_1
	5	3477 (17)	ν_1		5	3438 (11)	ν_1^{iso}
CH_4	1	3365 (8)	ν_1		6	3390 (12)	ν_1
	2	3369 (8)	ν_1		6	3440 (12)	ν_1^{iso}
					7	3394 (15)	ν_1
					7	3438 (14)	ν_1^{iso}

centers are listed in Table 1, together with their widths and assignments. The spectra for L = Ar and N_2 have been discussed in detail previously.[6,18,19] Thus, only the conclusions relevant to the present work are briefly summarized here.

1. L = Ar. The two bands observed for Ph^+-Ar are assigned to the ν_1 fundamentals of the H-bound ($\nu_1 = 3464$ cm^{-1}) and π-bound isomers ($\nu_1^{\pi} = 3536$ cm^{-1}) on the basis of the complexation-induced frequency shifts, band shapes, and the comparison with ab initio and density functional calculations.[18,19] The ν_1 band of H-bound Ph^+-Ar features a large redshift upon complexation ($\Delta\nu_1 = -70$ cm^{-1}),[19] an unambiguous signature of the formation of an intermolecular proton bond. In contrast, the weaker transition assigned to the π-bound isomer is almost unshifted ($\Delta\nu_1^{\pi} = +2$ cm^{-1}), indicating that the strength of the O−H bond is not affected by Ar complexation above the aromatic ring. The observed ν_1 band shapes confirm the given assignments. The ν_1 band of H-bound Ph^+-Ar is significantly shaded to the blue, due to the notable contraction of the intermolecular bond upon ν_1 excitation. The observed redshift of 70 cm^{-1} corresponds to the increase of the intermolecular interaction strength (on the order of 10%). On the other hand, the ν_1 band of π-bound Ph^+-Ar is nearly symmetric, as ν_1 excitation does not significantly change the intermolecular interaction. Ab initio calculations at the UMP2(fc)/6-311G-(2df,2pd) level of theory predict that H-bound Ph^+-Ar is the global minimum on the intermolecular potential energy surface ($D_e \approx 660$ cm^{-1}), whereas π-bound Ph^+-Ar is a less stable local minimum ($D_e \approx 400$ cm^{-1}).[18] The lowest-energy isomerization path from π-bound toward H-bound Ph^+-Ar is estimated to be above the phenolic C−O−H backbone with a barrier of ≈150 cm^{-1}.[19] Although the theoretical level underestimates somewhat the interaction strength (calculated $D_e \approx 400$ cm^{-1}, measured $D_0 = 535 \pm 3$ cm^{-1} for π-bound Ph^+-Ar), it is believed that the calculations correctly reproduce the topology of the interaction potential. Changes in the relative ν_1 band intensities and widths, induced by variations of the ion source conditions, clearly prove that π-bound Ph^+-Ar is less stable than H-bound Ph^+-Ar.[19] In addition, ZEKE spectra of π-bound Ph^+-Ar show regular vibrational structure assigned to an almost harmonic progression of the intermolecular bending mode up to 90 cm^{-1} ($n\nu_{bx} = 15$, 31, 46, 60, 74, and 89 cm^{-1} for $n = 1-6$),[5,7,8] confirming that the barrier for isomerization from the π-bound local minimum to the H-bound global minimum is indeed substantial (ν_{bx} is the bending vibration along the calculated lowest-energy isomerization path).

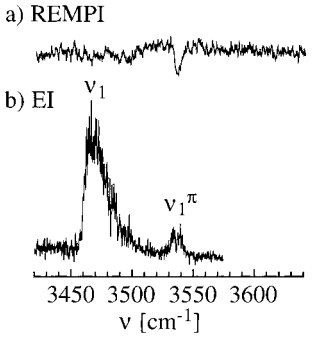

Figure 5. Comparison of the IR photodissociation spectra of Ph^+-Ar obtained when the cation cluster is produced by REMPI (a, reproduced from ref 17) or in the EI source (b). While both spectra show the ν_1 bands of the less stable π-bound isomer, the ν_1 band of the H-bound global minimum is only visible in spectrum b. The dip in the center of the ν_1^{π} band arises from atmospheric water absorptions along the IR laser path.

Figure 5 compares the IR spectra of Ph^+-Ar, where the cation clusters are produced either by REMPI (a, ref 17) or by EI (b). Whereas the EI-IR spectrum shows the ν_1 bands of both isomers, the REMPI-IR spectrum displays only the absorption of the less stable π-bound isomer.[6,17] The ν_1 absorption of the global minimum structure of Ph^+-Ar is completely missing in the REMPI-IR spectrum, clearly demonstrating the limitations of the REMPI ion source for the spectroscopic study of cation complexes. As π-bound Ph−Ar is the global potential minimum of the neutral species,[8] REMPI favors strongly the production of π-bound over H-bound Ph^+-Ar, owing to vertical transitions (FC principle, Figure 1, dashed arrows).[2,5−9,17] The population of the H-bound Ph−Ar appears to be small in usual expansions, probably because of a small isomerization barrier toward the π-bound global minimum.

2. L = He and Ne. Similar to Ph−Ar, Ph−He and Ph−Ne are expected to have π-bound equilibrium structures in their neutral ground states, and the analysis of the REMPI spectrum of Ph−Ne is compatible with this assumption (no spectroscopic data exist for Ph−He).[1] The IR spectra of Ph^+-He and Ph^+-Ne in Figure 4 display single bands centered at 3537 and 3534 cm^{-1}, with widths of 8 and 6 cm^{-1}, respectively. They occur close to the ν_1 transition of bare Ph^+, the center of which is reported as 3534 cm^{-1} (width, ≈10 cm^{-1}).[6] It is difficult to infer reliable experimental values for frequency shifts upon He and Ne complexation, as the widths of the observed transitions are larger than the shifts. Moreover, the Ph^+ and Ph^+-He/Ne absorptions are measured by different techniques. However, the band of Ph^+-Ne is clearly redshifted (by ≈3 cm^{-1}) compared

to the one of Ph^+-He (Figure 4). For π-bound geometries, the shift between Ph^+-Ne and Ph^+-He is expected to be smaller and to the other direction because the much more strongly bound π-bound Ph^+-Ar and Ph^+-Kr dimers show both a $1-2$ cm^{-1} blueshift with respect to bare Ph^+.[6,17−19] Consequently, it is concluded that the transitions in the Ph^+-He and Ph^+-Ne spectra mainly arise from ν_1 fundamentals of the H-bound structures, which are assumed to be the global minima on the respective intermolecular potentials. However, it cannot be completely excluded that part of the signal arises from the π-bound species, as their ν_1^{π} transitions are expected to occur in the same frequency range.

3. L = CH4. CH_4 is a nonpolar "spherical" ligand, and thus, its interaction with aromatic chromophores is expected to be similar to Ar (and other Rg ligands), with the major difference being that the larger polarizability of CH_4 leads to stronger interactions ($\alpha_L/4\pi\epsilon_0 = 1.63$ and 2.6 Å^3 for L = Ar and CH_4).[31] Hence, the topologies of the Ph−Ar and $Ph-CH_4$ potentials are expected to be similar (in all electronic states). Indeed, IR and REMPI spectra suggest that $Ph-CH_4$ has a π-bound equilibrium structure in S_0.[4,5] The vibrational and electronic band shifts of $Ph-CH_4$ are larger than that for Ph−Ar, confirming the stronger interaction in the former complex. The ZEKE spectrum of $Ph-CH_4$ reported in ref 5 corresponds almost certainly to vertical transitions into the π-bound minimum of the cation (Figure 1, dashed arrows). However, similar to Ph^+-Ar, the global minimum of Ph^+-CH_4 is expected to have a H-bound geometry. Indeed, the IR spectrum of Ph^+-CH_4 in Figure 4 shows a transition at 3365 cm^{-1}, which can be assigned to the ν_1 fundamental of H-bound Ph^+-CH_4. As expected, the redshift for CH_4 ($\Delta\nu_1 = -169$ cm^{-1}) is larger than that for Ar ($\Delta\nu_1 = -70$ cm^{-1}). The signal-to-noise ratio obtained for Ph^+-CH_4 is worse than that for Ph^+-Ar, owing to much larger background signals arising from MD and/or CID processes (section II). Thus, the ν_1 band of the π-bound structure, which is supposed to be a local minimum, could not be observed. The $Ph^+-(CH_4)_2$ spectrum discussed in section III.B is compatible with a H-bound equilibrium structure of Ph^+-CH_4.

4. L = N2. In contrast to Ph^+-Ar, the IR spectrum of Ph^+-N_2 in Figure 4 reveals only absorptions assigned to the H-bound structure, which is calculated to be the global minimum of the potential.[15,18] The redshift of the ν_1 fundamental ($\nu_1 = 3365$ cm^{-1}, $\Delta\nu_1 = -169$ cm^{-1}) is larger than that for Ph^+-Ar owing to the stronger intermolecular interaction. For the same reason, the head in the P-branch is more pronounced in the case of Ph^+-N_2. Two further weak bands are assigned to combination and sequence bands of ν_1 with the intermolecular stretching mode ($\nu_1 + \nu_s = 3484$ cm^{-1}, $\nu_1 + \nu_s - \nu_s = 3372$ cm^{-1}).[18] Such transitions are often observed for H-bound complexes.[20,21,32,33] The derived intermolecular stretching frequencies are $\nu_s = 113$ cm^{-1} in the intramolecular ground state (in good agreement with the value obtained from the ZEKE spectrum[14]) and 119 cm^{-1} in the ν_1 state. The larger ν_s frequency in the vibrationally excited state is compatible with the 169 cm^{-1} increase of the interaction from $D_0 = 1640 \pm 10$ cm^{-1} ($v_1 = 0$, ref 16) to 1809 ± 10 cm^{-1} ($v_1 = 1$). The spectrum shown in Figure 4 (as well as all other Ph^+-N_2 spectra recorded in the present work) does not display any spectroscopic signature of a π-bound Ph^+-N_2 isomer, which is predicted to be a less stable local minimum on the potential energy surface: the dissociation energies are estimated as $D_e = 1910$ and 771 cm^{-1} for H-bound and π-bound Ph^+-N_2 at the UMP2(fc)/6-311G(2df,2pd) level.[18] (The experimental value for H-bound Ph^+-N_2 is $D_0 = 1640 \pm 10$ cm^{-1}.[16]) Thus, the large difference in the stabilization energies and/or a low isomerization barrier from the π-bound toward the H-bound structure are responsible for the low population of the π-bound isomer in the molecular beam.

5. Comparison. a. Structures. From the preceding discussion, the following qualitative picture emerges. In the neutral ground state, S_0, Ph−L dimers have π-bound equilibrium structures for small closed-shell ligands without low-order static multipole moments (i.e., dipole and quadrupole). This is the case for L = Rg and L = CH_4, which interact with Ph mainly via their polarizability. Hence, dispersion interactions dominate the attraction in S_0 (induction is less important), and these can be maximized by close contact between L and the highly polarizable π-electron system of the aromatic ring. In the cation ground state, D_0, the positive charge gives rise to additional charge-induced dipole forces (the charge distribution of Ph^+ induces a dipole moment on the polarizable ligand). Apparently, the charge distribution of Ph^+ in the D_0 state strongly favors the H-bound over the π-bound geometry because the ligand L can closely approach the substantial positive partial charge centered on the acidic O−H proton. Thus, while Ph−Rg and $Ph-CH_4$ have π-bound global minima and H-bound local minima in S_0, the situation is reversed in D_0 (Figure 1).

In the case of small ligands with nonvanishing dipole and/or quadrupole moments (e.g., L = CO, N_2), Ph−L dimers prefer H-bonding over π-bonding even in S_0, owing to the electrostatic interaction of the permanent multipole moments of Ph (mainly the dipole moment) with those of L. Apparently, the dispersion forces (favoring the π-bound structure) are overridden by the electrostatic forces (favoring the H-bound structure) even for ligands with small dipole and/or quadrupole moments (such as CO and N_2). In the cation ground state, the electrostatic interactions become even more pronounced (due to the additional charge) so that Ph−L dimers with polar ligands have a H-bound equilibrium structure in both S_0 and D_0.

b. ν1 Frequencies and Bond Strengths. In H-bound $A-H^+-L$ dimers, the strength of the intermolecular bond depends on the difference in the proton affinities (PAs) of the two bases, A and L. As the PA of the phenoxy radical (873.2 kJ/mol)[34] exceeds by far the ones of all ligands discussed in this work (PA_L = 177.8, 198.8, 369.2, 493.8, and 543.5 kJ/mol for L = He, Ne, Ar, N_2, and CH_4, respectively),[35] the H-bound $C_6H_5O-H^+-L$ dimers are composed of a Ph^+ core that is slightly perturbed by the weak intermolecular bond to L. As PA_L is increased, the intermolecular bond becomes stronger and the proton becomes increasingly delocalized between C_6H_5O and L. This effect is reflected in the redshift of the O−H stretch frequency by complexation. Previous spectroscopic studies of $A-H^+-L$ dimers show that for a given base A the reduction of the A−H stretch frequency ($\Delta\nu_1$) scales linearly with PA_L.[21,36] Figure 6a reveals that this relation is also valid for the Ph^+-L dimers investigated in the present work. In addition, for a given L, the redshift is larger for bases A with lower PA: for example, $\Delta\nu_1 = -70$, -217, and -704 cm^{-1} for $C_6H_5OH^+-Ar$, $SiOH^+-Ar$,[20] and $OCOH^+-Ar$,[32] respectively, in line with $PA_{C_6H_5O} > PA_{SiO} > PA_{OCO}$ (873.2>777.8>540.5 kJ/mol).[34,35] It is noted that the O−H donor stretch frequencies could not accurately be measured for a variety of strongly H-bound Ph^+-L dimers, e.g., for ligands with a large dipole and/or quadrupole moment (such as L = H_2O, CH_3OH, C_6H_5OH, and C_6H_6),[37−40] because of very large shifts upon complexation and/or substantial broadening (several 100 cm^{-1}) arising from large couplings to the intermolecular degrees of freedom.

The attractive part of the intermolecular potential in H-bound Ph^+-Rg and Ph^+-CH_4 is mainly based upon the charge-

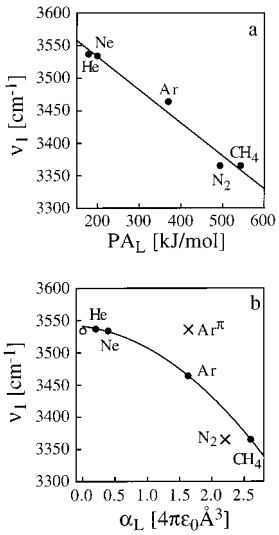

Figure 6. (a) Plot of the ν_1 frequency of various H-bound Ph^+-L dimers vs the proton affinity of L (L = He, Ne, Ar, CH_4, N_2). The line corresponds to a least-squares fit of the data points to a linear polynomial. (b) Plot of the ν_1 frequency of various H-bound Ph^+-L dimers vs the polarizability of L (L = He, Ne, Ar, CH_4). Also included are the data points for Ph^+ (open circle, ref 6), π-bound Ph^+-Ar and H-bound Ph^+-N_2 (crosses). The line corresponds to a least-squares fit of the data points of He, Ne, Ar, CH_4 (filled circles) to a second-order polynomial.

induced dipole interaction (V_{CID}) between the charge distribution in Ph^+ and the polarizability of the ligand, α_L. For a point charge, q, and a spherical polarizable ligand separated by a distance R, the induction interaction is given by $V_{CID} = -\alpha_L q^2/R^4$. The charge distribution in Ph^+ is only little affected by the weak interaction with L, and the intermolecular separation in Ph^+-L is roughly independent of L (for L = Rg and CH_4).[36] Consequently, the attractive V_{CID} potential and also the total interaction are expected to be roughly proportional to α_L. This relation has been confirmed by high-level ab initio calculations for a wide range of AH^+-Rg dimers composed of simple bases A (e.g., A = O, N_2, CO, CO_2, SiO) and the Rg atoms He, Ne, and Ar.[36,41] The dependence of the interaction strength in H-bound Ph^+-Rg and Ph^+-CH_4 upon α_L is also reflected in the ν_1 frequency, as demonstrated by the filled circles in Figure 6b. Similar to related AH^+-Rg systems,[36] the frequency drops slightly faster than linear with α_L ($\alpha_L/4\pi\epsilon_0$ = 0.20, 0.39, 1.63, and 2.6 Å^3 for L = He, Ne, Ar, and CH_4, respectively).[31] Extrapolation of $\alpha_L \rightarrow 0$ using a second-order polynomial yields $\nu_1 = 3542 \pm 4$ cm^{-1} for bare Ph^+. This value is slightly larger than the frequency reported in ref 6 ($\nu_1 = 3534 \pm 5$ cm^{-1}, open circle in Figure 6b). Also included in Figure 6b are the ν_1 frequencies of π-bound Ph^+-Ar and H-bound Ph^+-N_2 (as crosses). As expected, the data point of π-bound Ph^+-Ar deviates from the line for H-bound Ph^+-L because π-bonding has little effect on the phenolic O−H bond. The data point of Ph^+-N_2 deviates from the line owing to the nonvanishing quadrupole moment, which provides a further contribution to the interaction. Thus, although $\alpha_{N_2} < \alpha_{CH_4}$ ($\alpha_{||}/4\pi\epsilon_0$ = 2.20 Å^3 for N_2),[42] the interaction in Ph^+-N_2 and Ph^+-CH_4 appears to be comparable leading to similar values of $\Delta\nu_1$.

High-level ab initio calculations for determining accurate values for dissociation energies and structures of the Ph^+-L dimers are difficult to perform because of the large size and the open-shell character of Ph^+. Calculations for smaller cation dimers, such as NH_4^+-Rg, have shown that theoretical levels of at least MP2/aug-cc-pVTZ quality are required for a reliable description of the intermolecular potential.[20,41,43] As the PAs of NH_3 (853.6 kJ/mol)[35] and C_6H_5O (873.2 kJ/mol)[34] are comparable, the properties of the intermolecular bonds in H-bound NH_4^+-L and $C_6H_5OH^+-L$ dimers are expected to be similar. Ab initio calculations at the MP2/aug-cc-pVTZ level yield equilibrium geometries with linear proton bonds, dissociation energies of D_e = 145, 278, 927, and 2042 cm^{-1}, and intermolecular separations of R_e(H−L) = 2.10, 2.16, 2.31, and 2.00 Å for NH_4^+-L (L = He, Ne, Ar, N_2).[43,44] The anisotropy of the charge-quadrupole interaction favors a parallel alignment of the N_2 molecule and the intermolecular bond.[21,36] As PA_{NH_3} is slightly smaller than $PA_{C_6H_5O}$, the intermolecular bonds are expected to be slightly weaker and longer in the corresponding Ph^+-L dimers. Moreover, the asymmetry of Ph causes the intermolecular bonds in Ph^+-L to deviate slightly from linearity.[15,18] Calculations for the linear H-bound $SiOH^+-L$ dimers at the same level of theory yield D_e = 190, 332, 1117, and 2642 cm^{-1} and R_e(H−L) = 1.88, 1.95, 2.10, and 1.70 Å for L = He, Ne, Ar, and N_2.[36] Clearly, the interaction in $SiOH^+-L$ is significantly stronger than in NH_4^+-L and Ph^+-L owing to the smaller PA of SiO (777.8 kJ/mol).[35] The good agreement between theoretical and spectroscopic data observed for $SiOH^+-L$ and NH_4^+-L and the similar PAs of NH_3 and C_6H_5O provide confidence that the values given for NH_4^+-L approximate the corresponding Ph^+-L values reasonably well. Moreover, the binding energy of Ph^+-N_2 (measured as D_0 = 1640 ± 10 cm^{-1})[16] is consistent with D_e = 2042 cm^{-1} calculated for $NH_4^+-N_2$. From the comparison with NH_4^+-L, the dissociation energies of H-bound Ph^+-L are estimated to be on the order of $D_0 \approx$ 100, 250, 800, and 1600 cm^{-1} for L = He, Ne, Ar, and N_2.

B. Larger Ph^+-L_n Clusters ($n > 1$). Figure 7 compares the IR photodissociation spectra of $Ph^+-(N_2)_n$ (n = 1−7), Ph^+-Ar_n (n = 1−5), and $Ph^+-(CH_4)_n$ (n = 1,2) in the range of the ν_1 vibration of Ph^+. The observed band centers are listed in Table 1, together with their widths and assignments. All spectra are dominated by a strong transition, which is assigned to the ν_1 fundamental of the most stable isomer of each cluster ion. The positions of these bands are plotted in Figure 8 as a function of the cluster size for L = N_2 and Ar. As discussed in section III.A, the ν_1 bands of the most stable dimers are significantly redshifted with respect to the monomer transition because of the formation of the proton bond. Further complexation causes in all cases only small incremental blueshifts, $\Delta\nu_1(n) = \nu_1(n) - \nu_1(n-1)$, indicating that the influence of these ligands on the strength of the O−H bond is small. The shifts for Ar are $\Delta\nu_1(n) \approx 2-5$ cm^{-1} for n = 2−5. The shifts are larger for N_2, $\Delta\nu_1(n) \approx 3-10$ cm^{-1} for n = 2−7, as a consequence of the stronger interaction. In general, the incremental shifts tend to become smaller for increasing n, although they are not converged to zero at the largest cluster sizes investigated. Unfortunately, there appear to be no matrix isolation studies of Ph^+ in argon or nitrogen, making it impossible at this stage to compare the cluster data with the bulk limit.

The large redshifts for the H-bound dimers arise from the destabilization of the intramolecular O−H bond upon formation of the intermolecular proton bond. The small incremental blueshifts for $n > 1$ indicate that further solvation of the H-bound dimer core leads to a slight increase of the O−H bond strength, which is accompanied by a weakening of the intermolecular proton bond to the first ligand. In the case of $Ph^+-(N_2)_n$ (n = 1,2), this effect is also visible in the intermolecular stretching frequencies in the ν_1 state derived from

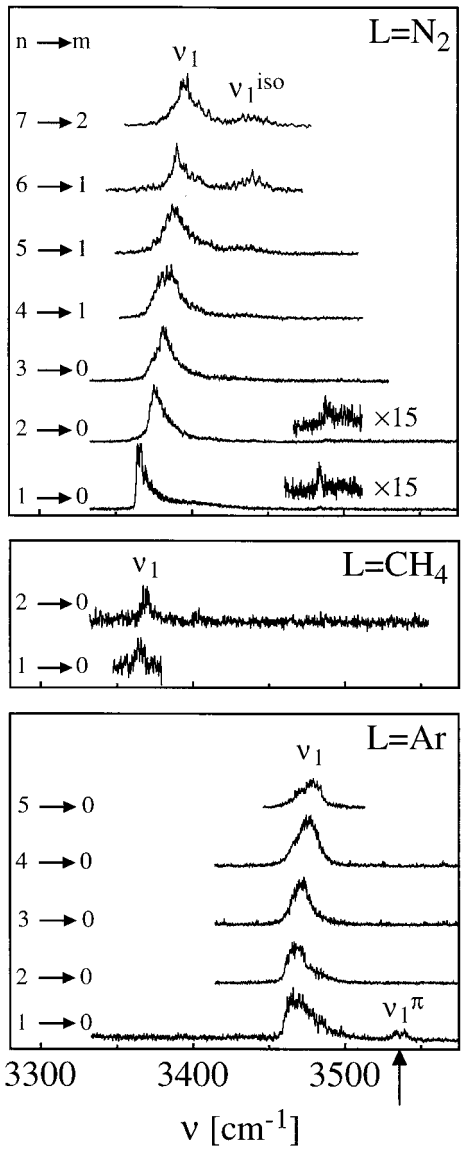

Figure 7. IR photodissociation spectra of Ph^+-L_n ($L = N_2$, CH_4, Ar) recorded in the dominant Ph^+-L_m fragment channel (indicated as $n \rightarrow m$). The strongest band in each spectrum is attributed to the ν_1 fundamental of the most stable isomer. For Ph^+-Ar, the ν_1 transition of the less stable π-bound isomer is indicated as ν_1^{π}. In the case of $Ph^+-(N_2)_n$, with $n \geq 5$, also a ν_1 band attributed to a less stable isomer is observed (ν_1^{iso}). Part of the $Ph^+-(N_2)_{1,2}$ spectra are expanded by a factor 15 to show the weak $\nu_1 + \nu_s$ transitions. The arrow indicates the ν_1 frequency of bare Ph^+ ($\nu_1 = 3534$ cm^{-1}).

the weak $\nu_1 + \nu_s$ combination bands (at 3484 and 3488 cm^{-1}, Table 1, Figure 7). The ν_s mode corresponds to the intermolecular stretching vibration of the H-bound ligand, and its frequency decreases from 119 ($n = 1$) to 113 cm^{-1} ($n = 2$). The fact that the ν_s frequencies (and also intensities) are similar for $n = 1$ and 2 shows that both the geometry and strength of the nearly linear proton bond are not significantly changed upon complexation with the second ligand. In general, the spectral signatures of the microsolvation of Ph^+ in Ar and N_2 are very similar to those observed previously for related AH^+-L_n systems having a single acid proton, such as OCH^+-Ar_n,[24] $SiOH^+-Ar_n$,[20] $N_2H^+-Ar_n$,[25] and $N_2H^+-Ne_n$.[26]

In addition to the H-bond, which corresponds to the global minimum on the potential of all considered Ph^+-L dimers, there are several less stable binding sites for further solvation. For example, ligands can be attached to the π-electron system of the aromatic ring (π-bond), to one or two neighboring H atoms of the ring (linear or bridged H^C-bond), to the O atom (O-bond), or to the O−H proton (to fill an equatorial ring around the nearly linear O−H−L proton bond, H^R-bond). Whereas π-bonds and H^C-bonds are expected to have only little influence on ν_1, significant shifts may be expected for O-bonds and H^R-bonds.

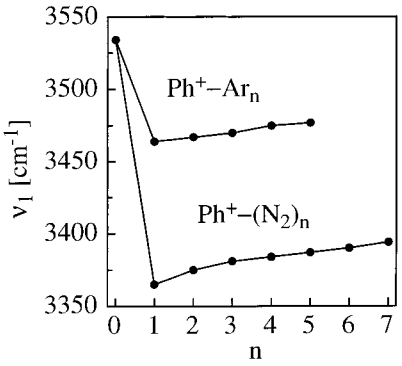

Figure 8. Plot of the ν_1 frequencies of the most stable isomers of Ph^+-Ar_n and $Ph^+-(N_2)_n$ as a function of the cluster size (n).

In the case of Ph^+-Ar, ab initio calculations at the UMP2-(fc)/6-311G(2df,2pd) level suggest that O-bonds and H^R-bonds (both $D_e \approx 250$ cm^{-1}) are less stable than the positions above the aromatic ring ($D_e \approx 250-400$ cm^{-1}).[19] Consequently, it is assumed that the most stable Ph^+-Ar_n geometries are those in which the first ligand forms a H-bond and further ligands are attached to the aromatic ring to form π-bonds and/or H^C-bonds: calculations at the UMP2(fc)/6-31G* level predict similar binding energies for π-bound and linear H^C-bound Ph^+-Ar dimers. As discussed in section III.A.1, the weak band observed in the Ph^+-Ar spectrum is consistent with an assignment to a π-bound structure (ν_1^{π}, Figure 5). The fact that this absorption disappears in the spectra of larger Ph^+-Ar_n clusters confirms that this binding site is a local (and not the global) minimum on the dimer potential. Consequently, the Ph^+-Ar_2 trimer with a (1|1) structure (C_s symmetry) observed in PIE spectra[2] does not correspond to the global minimum structure (although it is the most stable structure of the neutral species),[2,28] again demonstrating the limitations of REMPI ion sources for the spectroscopy of cluster ions. The absence of the absorption attributed to ν_1^{π} in the spectra of larger Ph^+-Ar_n clusters (Figure 7) excludes an assignment of this band to $\nu_1 + \nu_s$ of the H-bound dimer (such bands are observed for $L = N_2$). The spectra of $Ph^+-(CH_4)_{1,2}$ suggest that the sequence of the cluster growth in $Ph^+-(CH_4)_n$ is similar to that of Ph^+-Ar_n.

The main features in the spectra of $Ph^+-(N_2)_n$ are similar to those of Ph^+-Ar_n, except that the observed shifts are larger because of the stronger interactions. Thus, it is assumed that in the most stable $Ph^+-(N_2)_n$ structures the H-bound dimer is further solvated at the aromatic ring. As discussed in section III.A.4, the π-bound local minimum is not observed for Ph^+-N_2. The incremental blueshifts for $n = 2$ and 3 (10 and 6 cm^{-1}) are significantly larger than those for $n > 3$ (3−4 cm^{-1}). This may be taken as evidence for the following tentative cluster growth model: the second and third N_2 ligands are attached to opposite sites of the aromatic ring (π-bonds), leading to a (1|1) configuration for $Ph^+-(N_2)_3$ and significant blueshifts; further ligands form equivalent H^C-bonds, causing the somewhat smaller but constant blueshift. Interestingly, the spectra of $Ph^+-(N_2)_n$ with $n = 5-7$ display weaker bands shifted to the blue (by $\approx$50 cm^{-1}) of the ν_1 bands of the most stable structures. They are tentatively attributed to ν_1 bands of less stable isomers (ν_1^{iso}) where one N_2 ligand is attached to the O−H proton to form a

TABLE 2: Photofragmentation Branching Ratios (in %) of Ph^+-L_n Complexes for the Photoinduced Reaction in Eq 2 Measured at the Band Maxima of the ν_1 Fundamental[a]

L	n	$m=0$	$m=1$	$m=2$
He, Ne	1	100		
Ar	1−4	100		
	5	95	5	
CH_4	1, 2	100		
N_2	1, 2	100		
	3	90	10	
	4	5	95	
	5	5	95	
	6	10	55	35
	7		15	85

[a] Only channels contributing more than 5% are listed. Uncertainties are estimated as 5%.

H^R-bond. Complexation at this position is expected to have a substantial influence on the O−H stretch frequency, in agreement with the experimental observations. Moreover, calculations at the B3LYP/6-31G* level predict a significant blueshift for H^R-bonding.

Table 2 summarizes the photofragmentation branching ratios measured for resonant excitation of the ν_1 transition of the most stable structures of Ph^+-L_n (eq 2). Similar to previous studies of related systems the observed range of fragment channels is rather narrow.[20,22−27,45] This information can be used to roughly estimate incremental ligand binding energies, assuming a statistical model for the evaporation process after IR excitation and the following approximations: (i) the difference in the internal energies of the parent cluster and the fragmentation products as well as the kinetic energy release are neglected; (ii) only single ligands and no larger L_k oligomers are evaporated; (iii) ligands with smaller binding energies are evaporated first; (iv) three-body forces are assumed to be small. According to this simple model, the absorbed photon energy (single photon absorption) can be used for ligand evaporation. Moreover, ligands at the same binding sites are assumed to have the same binding energies. For the following rough estimation, the ligands are classified into H-bound and π-bound ones (it is recalled that π-bonds and H^C-bonds have comparable calculated binding energies for L = Ar and N_2). In addition, the dissociation energies of π-bound Ph^+-Ar (535 ± 3 cm^{-1}) and H-bound Ph^+-N_2 (1640 ± 10 cm^{-1}) determined from MATI spectroscopy are used.[9,16]

The fact that the vibrational energy of $\nu_1 = 3477$ cm^{-1} is sufficient to evaporate all ligands in Ph^+-Ar_5 (one H-bound and four π-bound ligands, Table 2) gives rise to an upper limit of $D_0 < 1340$ cm^{-1} for H-bound Ph^+-Ar. From the comparison with the dissociation energy of NH_4^+-Ar ($D_0 \approx 825$ cm^{-1}),[23] which is expected to have a slightly stronger bond (section III.A.5.b), the upper limit may be reduced to 800 cm^{-1}. A lower limit for H-bound Ph^+-Ar is given by $D_0 = 535$ cm^{-1} of π-bound Ph^+-Ar, which is certainly a less stable isomer. Thus, the dissociation energy of H-bound Ph^+-Ar is estimated as 535 cm^{-1} < D_0 < 800 cm^{-1}, compatible with the value calculated at the UMP2(fc)/6-311(2df,2pd) level, $D_e = 656$ cm^{-1}.[18] In the case of $Ph^+-(N_2)_n$ clusters, the photofragmentation ratios yield 600 cm^{-1} < D_0 < 900 cm^{-1} for π-bound (and/or H^C-bound) Ph^+-N_2, again in agreement with the calculated value (D_e = 771 cm^{-1}, UMP2(fc)/6-311(2df,2pd) level).[18] Thus, the π-bound structure of Ph^+-N_2 is substantially less stable than the H-bound structure (by $\approx 10^3$ cm^{-1}), consistent with the absence of the π-bound isomer in the dimer spectrum (Figure 4). In contrast, the difference in the binding energies of both isomers is much smaller for Ph^+-Ar (<300 cm^{-1}), giving rise to the observation of both species in the IR spectrum (recorded with the EI source, Figure 5). The very similar redshifts of H-bound Ph^+-CH_4 and Ph^+-N_2 suggest that their binding energies are comparable, leading to a D_0 value on the order of 1500 cm^{-1} for H-bound Ph^+-CH_4. The dissociation energy of π-bound Ph^+-CH_4 can be approximated by the value obtained for π-bound $C_6H_6^+-CH_4$ ($D_0 \approx 1000$ cm^{-1}) estimated from photofragmentation data.[45] In analogy to Ph^+-Ar, π-bound Ph^+-CH_4 is less stable than H-bound Ph^+-CH_4. Moreover, the derived binding energies of the two Ph^+-CH_4 isomers are compatible with the experimental observation that resonant excitation of ν_1 of $Ph^+-(CH_4)_2$ at 3369 cm^{-1} is sufficient to break both intermolecular bonds (one H-bond and one π-bond).

IV. Concluding Remarks

IR photodissociation spectra of a variety of Ph^+-L_n (L = He, Ne, Ar, CH_4, N_2) complexes are presented in the vicinity of the O−H stretch (ν_1) vibration of the electronic ground state of Ph^+. Analyses of the size-dependent complexation-induced frequency shifts ($\Delta\nu_1$) and photofragmentation branching ratios provide valuable insight into the microsolvation of Ph^+ in nonpolar environments. All spectra are dominated by the ν_1 fundamental of the most stable isomer of each cluster cation. The dimers ($n = 1$) have H-bound equilibrium structures, a conclusion derived from the observed linear correlation between the proton affinity of L and the large redshifts ($\Delta\nu_1$). The strong correlation between $\Delta\nu_1$ and the polarizability of nonpolar ligands (L = Rg, CH_4) is taken as evidence that charge-induced dipole interactions dominate the attraction in these dimers. In the case of Ph^+-N_2, additional electrostatic forces arising from the nonvanishing quadrupole moment of N_2 (charge-quadrupole interaction) increase the intermolecular attraction. Small incremental blueshifts of ν_1 in the spectra of larger clusters ($n > 1$) indicate that further solvation of the H-bound dimers occurs at the aromatic Ph ring. For several clusters, less stable isomers are identified. In general, the signatures of the cluster growth of Ph^+-L_n are very similar to those observed previously for related AH^+-L_n clusters. The present study demonstrates that the combination of IR spectroscopy and mass spectrometry provides a sensitive probe of structures, binding energies, and the type of interaction in cluster ions.

An important aspect of the experimental strategy applied in the present work is the production of Ph^+-L_n complexes in an EI cluster ion source rather than by resonant photoionization techniques (REMPI). The EI ion source produces predominantly the most stable isomer of a given cluster ion. In contrast, the REMPI ion source generates preferentially that isomer of the cluster ion which has a structure similar to the neutral precursor (FC principle). As the type and strength of the interactions are quite different in the neutral and cation cluster, they often have quite different equilibrium geometries. Examples include Ph−Rg and Ph−CH_4 which prefer π-bonding in the neutral cluster but H-bonding in the cation cluster. In these cases, the spectra of Ph^+-L dimers observed by REMPI techniques do not correspond to the most stable structures (see Figure 5). For example, the derived ionization energies in ZEKE, MATI, and PIE spectra do not correspond to the adiabatic ionization energies. Similar conclusions hold also for larger cluster systems (e.g., Ph^+-Ar_2). Finally, it is noted that cluster ion sources have been used which utilize REMPI to selectively ionize the Ph monomer (and not the $Ph-L_n$ complex) before cluster formation occurs in the expansion. Similar to the EI source, such REMPI sources favor the production of the most stable structure of a given Ph^+-L_n cation.[40]

Acknowledgment. This study is part of Project No. 20-55285.98 of the Swiss National Science Foundation. O.D. was introduced into the field of ion−ligand interactions during his PhD work with E. W. Schlag at the Technical University of Munich (1991−1994). He would like to thank him for the very stimulating discussions during that time, in particular about the properties of phenol cation complexes.

References and Notes

(1) Mons, M.; Le Calve, J.; Piuzzi, F.; Dimicoli, I. *J. Chem. Phys.* **1990**, *92*, 2155.
(2) Gonohe, N.; Abe, H.; Mikami, N.; Ito, M. *J. Phys. Chem.* **1985**, *89*, 3642.
(3) Bieske, E. J.; Rainbird, M. W.; Atkinson, I. M.; Knight, A. E. W. *J. Chem. Phys.* **1989**, *91*, 752.
(4) Hartland, G. V.; Henson, B. F.; Venturo, V. A.; Felker, P. M. *J. Phys. Chem.* **1992**, *96*, 1164.
(5) Zhang, X.; Knee, J. L. *Faraday Discuss.* **1994**, *97*, 299.
(6) Fujii, A.; Miyazaki, M.; Ebata, T.; Mikami, N. *J. Chem. Phys.* **1999**, *110*, 11125.
(7) Haines, S. R.; Dessent, C. E. H.; Müller-Dethlefs, K. *J. Electron Spectrosc. Relat. Phenom.* **2000**, *108*, 1.
(8) Dessent, C. E. H.; Müller-Dethlefs, K. *Chem. Rev.* **2000**, *100*, 3999.
(9) Dessent, C. E. H.; Haines, S. R.; Müller-Dethlefs, K. *Chem. Phys. Lett.* **1999**, *315*, 103.
(10) Klopper, W.; Lüthi, H. P.; Brupbacher, T.; Bauder, A. *J. Chem. Phys.* **1994**, *101*, 9747.
(11) Hobza, P.; Selzle, H. L.; Schlag, E. W. S. *Chem. Rev.* **1994**, *94*, 1767.
(12) Neusser, H. J.; Krause, H. *Chem. Rev.* **1994**, *94*, 1829.
(13) Brupbacher, T.; Makarewicz, J.; Bauder, A. *J. Chem. Phys.* **1994**, *101*, 9736.
(14) Haines, S. R.; Geppert, W. D.; Chapman, D. M.; Watkins, M. J.; Dessent, C. E. H.; Cockett, M. C. R.; Müller-Dethlefs, K. *J. Chem. Phys.* **1998**, *109*, 9244.
(15) Chapman, D. M.; Müller-Dethlefs, K.; Peel, J. B. *J. Chem. Phys.* **1999**, *111*, 1955.
(16) Haines, S. R.; Dessent, C. E. H.; Müller-Dethlefs, K. *J. Chem. Phys.* **1999**, *111*, 1947.
(17) Fujii, A.; Sawamura, T.; Tanabe, S.; Ebata, T.; Mikami, N. *Chem. Phys. Lett.* **1994**, *225*, 104.
(18) Solcà, N.; Dopfer, O. *Chem. Phys. Lett.* **2000**, *325*, 354−359.
(19) Solcà, N.; Dopfer, O. *J. Mol. Struct.*, in press.
(20) Olkhov, R. V.; Nizkorodov, S. A.; Dopfer, O. *Chem. Phys.* **1998**, *239*, 393.
(21) Bieske, E. J.; Dopfer, O. *Chem. Rev.* **2000**, *100*, 3963.
(22) Dopfer, O.; Roth, D.; Maier, J. P. *J. Phys. Chem. A* **2000**, *104*, 11702.
(23) Dopfer, O.; Nizkorodov, S. A.; Meuwly, M.; Bieske, E. J.; Maier, J. P. *Int. J. Mass Spectrom. Ion Processes* **1997**, *167−168*, 637.
(24) Nizkorodov, S. A.; Dopfer, O.; Ruchti, T.; Meuwly, M.; Maier, J. P.; Bieske, E. J. *J. Phys. Chem.* **1995**, *99*, 17118.
(25) Dopfer, O.; Olkhov, R. V.; Maier, J. P. *J. Phys. Chem. A* **1999**, *103*, 2982.
(26) Nizkorodov, S. A.; Meuwly, M.; Maier, J. P.; Dopfer, O.; Bieske, E. J. *J. Chem. Phys.* **1998**, *108*, 8964.
(27) Olkhov, R. V.; Nizkorodov, S. A.; Dopfer, O. *J. Chem. Phys.* **1998**, *108*, 10046.
(28) Schmidt, M.; Mons, M.; Le Calve, J. *Z. Phys. D* **1990**, *17*, 153.
(29) Bieske, E. J. *J. Chem. Soc., Faraday Trans.* **1995**, *91*, 1.
(30) Guelachvili, G.; Rao, K. N. *Handbook of Infrared Standards*; Academic Press: London, 1993.
(31) Israelachvili, J. *Intermolecular and Surface Forces*; Academic Press: London, 1992.
(32) Dopfer, O.; Olkhov, R. V.; Roth, D.; Maier, J. P. *Chem. Phys. Lett.* **1998**, *296*, 585.
(33) Dopfer, O.; Nizkorodov, S. A.; Olkhov, R. V.; Maier, J. P.; Harada, K. *J. Phys. Chem. A* **1998**, *102*, 10017.
(34) Kim, H.; Green, R. J.; Qian, J.; Anderson, S. L. *J. Chem. Phys.* **2000**, *112*, 5717.
(35) Hunter, E. P. L.; Lias, S. G. *J. Phys. Chem. Ref. Data* **1998**, *27*, 413.
(36) Olkhov, R. V.; Dopfer, O. *Chem. Phys. Lett.* **1999**, *314*, 215.
(37) Fujii, A.; Iwasaki, A.; Yoshadi, K.; Ebata, T.; Mikami, N. *J. Phys. Chem. A* **1997**, *101*, 1798.
(38) Sawamura, T.; Fujii, A.; Sato, S.; Ebata, T.; Mikami, N. *J. Phys. Chem. A* **1996**, *100*, 8131.
(39) Kleinermanns, K.; Janzen, C.; Spangenberg, D.; Gerhards, M. *J. Phys. Chem. A* **1999**, *103*, 5232.
(40) Ebata, T.; Fujii, A.; Mikami, N. *Int. J. Mass Spectrosc. Ion Processes* **1996**, *159*, 111.
(41) Dopfer, O. *J. Phys. Chem. A* **2000**, *104*, 11693.
(42) Gray, C. G.; Gubbins, K. E. *Theory of Molecular Fluids*; Clarendon: Oxford, 1984; Vol. 1.
(43) Lakin, N. M.; Dopfer, O.; Meuwly, M.; Howard, B. J.; Maier, J. P. *Mol. Phys.* **2000**, *98*, 63.
(44) Dopfer, O. et al. Unpublished results.
(45) Dopfer, O.; Olhov, R. V.; Maier, J. P. *J. Chem. Phys.* **1999**, *111*, 10754.